Multi-region active contours
with a single level set function

Anastasia Dubrovina, Guy Rosman, and Ron Kimmel, *Fellow, IEEE*

Abstract—Segmenting an image into an arbitrary number of coherent regions is at the core of image understanding. Many formulations of the segmentation problem have been suggested over the past years. These formulations include, among others, axiomatic functionals, which are hard to implement and analyze, and graph-based alternatives, which impose a non-geometric metric on the problem.
We propose a novel method for segmenting an image into an arbitrary number of regions using an axiomatic variational approach. The proposed method allows to incorporate various generic region appearance models, while avoiding metrication errors. In the suggested framework, the segmentation is performed by level set evolution. Yet, contrarily to most existing methods, here, multiple regions are represented by a single non-negative level set function. The level set function evolution is efficiently executed through the *Voronoi Implicit Interface Method* for multi-phase interface evolution. The proposed approach is shown to obtain accurate segmentation results for various natural 2D and 3D images, comparable to state-of-the-art image segmentation algorithms.

Index Terms—Segmentation, multi-region, active contours, level sets

✦

Fig. 1. Multi-region image segmentation.

1 INTRODUCTION

IMAGE segmentation plays an important role in various areas of image processing, such as object detection and classification, action classification, scene understanding, and other visual information analysis processes. Existing algorithms for image segmentation may be broadly divided into several groups according to the following criteria: automatic segmentation vs. user-assisted approaches, object and background segmentation vs. multi-region segmentation, types of segmentation criteria, usage of prior data, such as various segment statistics or known shape priors, algorithms using a discrete optimization vs. a continuous one, etc.

In this paper we consider the active contours ap-

• A. Dubrovina and R. Kimmel are with the Department of Computer Science, Technion - Israel Institute of Technology, Haifa, 32000, Israel.
E-mail: nastyad@cs.technion.ac.il, ron@cs.technion.ac.il
• G. Rosman is with Computer Science and Artificial Intelligence Laboratory, MIT, Cambridge, MA, USA.
E-mail: rosman@csail.mit.edu

proach to image segmentation, which may be traced back to the snake model of [1]. In the active contours approach, region boundaries are modelled by a (parametric) curve, which minimizes the chosen type of segmentation criterion modelled as an energy functional. Important advantage of the active contours approach is the ability to minimize arbitrary energy functionals, while allowing for accurate region boundary detection with subpixel precision. The active contours approaches may be loosely classified into edge-based methods [1], [2], [3], [4], region-based methods [5], [6], [7], and combined approaches [8], [9], [10], to mention just a few.

Other common approaches to multi-region image segmentation either use a discrete labeling problem formulation and solve it using graph-cuts [13], [14], [15], or minimize the segmentation functional using convex relaxation techniques [16], [17], [18], [19], [20]. Contrary to the active contours method, such approaches require more effort to adapt for arbitrary segmentation functionals, in terms of both data and geometry priors, and usually require knowing the number of regions a priori, with the notable exception of [11], [12]. Other methods for multi-region image segmentation include mean-shift clustering [21], spectral segmentation [22], greedy algorithms [23], learning approaches [24], [25], and a combination of the above [26].

Compared to the above methods, the level set framework provides a significant amount of flexibility in the design of the segmentation criterion, and can be naturally extended to accommodate various assumptions about the image and its structure. These assumptions include different appearance models [7], [27], [28], [29], and shape priors [30], [31], [32].

The active contour evolution is commonly performed using the level set approach of [33], as in [2], [34], [35], [4]. The conventional level set framework is geared towards two-region image segmentation. Various methods were developed to alleviate this limitation; most of them require managing *multiple* level set functions. Some methods associate a level set function with each image region, and evolve these functions in a coupled manner, so that the resulting regions do not develop gaps or overlaps [36], [37], [38]. Other method perform hierarchical segmentation, by iteratively splitting previously obtained regions using the conventional level set framework [39], [40]. A different method was suggested by [41], where a smaller number of n level set functions were used to segment an image into 2^n regions.

Several approached were suggested, where a single level set function is used to perform the level set evolution, similar to the method introduced in the present paper. One such approach was recently suggested in [42]. While using a single level set function to represent image regions, it still requires managing multiple auxiliary level set functions when evolving the contour, so that no gaps/overlaps are created. In [16], [43], partitioning an image into multiple regions was modelled by a single, piecewise constant level set function, which was obtained using either augmented lagrangian optimization, or graph-cuts. However, these methods were designed to minimize the piecewise constant Mumford-Shah functional [5] only, though they may possibly be extended for more elaborated image appearance models.

Here, we propose a new level set method for multi-region image segmentation, where the regions are represented by a single non-negative level set function, such that the zero level set of this function corresponds to the region boundaries. The proposed method allows segmenting images with arbitrary number of regions using various image appearance models. To perform the level set evolution, the suggested method utilizes a novel level set framework for multi-phase interface evolution - the Voronoi Implicit Interface Method (VIIM), which was introduced by Saye and Sethian in [44], [45], for numerical simulations of fluid dynamics. During the evolution, performed using the foremention non-negative level set function, the VIIM implicitly deals with regions merging and splitting, and naturally handles complex topological structures such as triple junctions.

The main contributions of the present paper can be summarized as follows: first, we review the axiomatic formulation of the multi-region image segmentation problem as an energy functional minimization. We consider the region competition model of [8] and the pairwise dissimilarity-based models of [46], [47], augmented with the geodesic active contour regularization term [4], as our energy functionals. We then show the derivation of the steepest descent minimization for

the proposed functionals for multi-region segmentation. We formulate the active contour evolution equation as a multi-region level set evolution problem, and solve it by utilizing the VIIM level set framework. In the proposed method, neither the number of regions, nor the region statistics are required to be known a priory, and good segmentation results are produced for various initial conditions, extending the method presented in [48].

The structure of the paper is as follows: in Section 2 we describe the multi-region segmentation model, and the prominent segmentation priors that fit within the suggested framework. In Section 3 we review the level set approach for active contour evolution, and the Voronoi Implicit Interface Method, which is the numerical basis for our approach. In Section 4 we describe the main ideas that underlie the proposed method, derive the corresponding level set evolution equation in terms of the VIIM framework, and discuss implementation considerations. In Section 5 we present segmentation results and qualitative evaluation of the proposed approach, and compare it to state-of-the-art methods. Section 6 concludes the paper.

2 PROBLEM DEFINITION

Given an image $I(x)$ defined over a domain $\Omega \in \mathbb{R}^2$, the active contour model finds a contour $C(s) = (x_1(s), x_2(s)) \in \Omega$ that minimizes an energy functional of the type

$$E(C) = E_{data}(C) + \mu E_{reg}(C). \qquad (1)$$

The data term $E_{data}(C)$ is determined by the region-based image intensity model, for instance, piecewise smooth or piecewise constant model [5] and [6], pairwise region interaction model [7], [27], [49], [46], etc. The regularization term $E_{reg}(C)$ is determined by the segmenting contour properties. It may depend on the contour length alone [1], [5], [6], or incorporate image information, as is the case for the geodesic active contour model [34], [4].

The above energy functional is typically minimized by steepest descent with respect to the virtual arbitrary time parameter t, to obtain the optimal partition of the image

$$C_t = -\frac{\delta E(C)}{\delta C} = -\left[\frac{\delta E_{data}(C)}{\delta C} + \mu \frac{\delta E_{reg}(C)}{\delta C} \right]. \qquad (2)$$

In this paper we demonstrate region-based terms that rely on two specific image models - variants of the region-competition model of [8], namely the piecewise-constant model of [5], [6] and a more general *Gaussian mixture model* (GMM), and the pairwise dissimilarity model suggested in [49], [46]. Below we describe in details both models, formulated for multi-region segmentation, and the corresponding curve evolution rules.

In the case of volumetric image segmentation, the image $I(x)$ is defined over a domain $\Omega \subset \mathbb{R}^3$, and the segmentation is performed using the active surface model (see, for instance, [35], [50]), with similar problem formulation. To keep the notations simple, we first proceed by discussing the 2D problem, and describe the 3D case in more detail in Section 4.2.

2.1 Region-competition model

The energy functional In this paper we consider the region competition model of Zhu and Yuille [8], which we augment with geodesic active contour (GAC) [4] regularization term

$$E(C, \{\alpha_i\}) = \sum_{i=1}^{M} \int_{\Omega_i} -\log P\left(I(x)|\alpha_i\right) dx$$
$$+ \frac{\mu}{2} \sum_i \oint_{C_i} g(C_i(s)) ds, \qquad (3)$$

where $x \in \Omega$ denotes a point in the image domain. The model attempts to divide the domain Ω into a series of M non-overlapping regions $\{\Omega_i\}_{i=1}^{M}$, such that $\Omega = \{\cup_{i=1}^{M} \Omega_i\}$, with homogeneous intensities. Image intensity homogeneity is measured by the data term, where $P(z|\alpha_i)$ is the probability distribution function describing the image intensity values in the region Ω_i, having corresponding parameters α_i. The curve $C_i(s)$, parameterized by the arclength s, denotes the boundary of the region Ω_i, and can also be defined as $C_i = \partial\Omega_i$. Each boundary $C_i(s)$ is parameterized to have a counter-clockwise direction with respect to its corresponding region Ω_i. The contour C is given by union of all C_i, $C = \bigcup_i C_i$.

The regularization term is defined using an inverse edge indicator function $g(x)$. Here, we used $g(x) = \left(1 + |\nabla(G*I)|^2\right)^{-1}$, as suggested in [4], though other indicator functions may be considered. For color or vector valued images, one may use the edge indicator functions suggested in [10] or [51]. [10] treats the image as a 5-dimensional manifold (for color images) with metric $g_{\mu\nu}(x)$, and define $g = \det(g_{\mu\nu}(x))^{-1}$, while [51] uses the largest eigenvalue of the metric tensor, λ, and define $g = (1+\lambda^2)^{-1}$. The regularization term is multiplied by a factor $1/2$ as every boundary segment appears in Eq. (3) twice. Note that the proposed formulation is general and may be applied with various image intensity probability distribution models, as will be demonstrated in Sect. 2.2.

Optimization The energy functional $E(C, \{\alpha_i\})$ depends on both the contour C and the probability distribution parameters $\{\alpha_i\}$. To minimize the energy with respect to these two sets of variables, an alternating minimization approach is commonly used. First, for a fixed contour C and the partition $\{\Omega_i\}$, minimize the energy with respect to the parameters $\{\alpha_i\}$. Or,

equivalently, compute the optimal parameters maximizing the image probability in each region

$$\alpha_i^* = \arg\max_{\alpha_i} \prod_{x \in \Omega_i} P(\alpha_i|I(x)), \quad \forall i. \qquad (4)$$

Next, for fixed parameters $\{\alpha_i\}$, do a steepest descent step to compute the new contour C

$$C_t = -\frac{\delta E}{\delta C}$$
$$= \sum_{i \in N(x)} \left[-\log P\left(I(x)|\alpha_i\right) + \frac{\mu}{2}\left(\kappa_i g - \langle \nabla g, \mathbf{n}_i \rangle\right) \right] \mathbf{n}_i. \qquad (5)$$

In the above equation, consider some $x \in C$. The set $N(x)$ is comprised of the indices of the regions Ω_j adjacent to C at x. The curvature κ_i and the normals $\mathbf{n}_i$ correspond to the region boundaries Ω_i, when the normal $\mathbf{n}_i$ is defined such that it points inwards the region Ω_i. For a point x lying on a contour segment defining a boundary between two regions Ω_i and Ω_j, we have $|N(x)| = 2$, while for a triple junction point we have $|N(x)| = 3$.

The minimizing flow (5) is obtained by differentiating the energy functional $E(C)$ with respect to the active contour C. The first term was derived in [8], while the second term is the explicit geodesic active contour flow [4], obtained by differentiating the regularization term in Eq. (3).

2.2 Region competition model: examples

A piecewise constant model [5], [6] is a special case of the region competition model. Assuming Gaussian probability distributions, given by $I \sim \mathcal{N}(c_i, \sigma_i^2)$ in a region Ω_i, with identical variances $\sigma_i = \sigma_j, \forall i, j$, the data term of the energy functional $E(C)$ becomes

$$E_{data}(C, \{c_i\}) = \sum_{i=1}^{M} \int_{\Omega_i} (I(x) - c_i)^2 dx. \qquad (6)$$

The above equation describes the piecewise constant variant of the Mumford-Shah energy functional [5]. For $M = 2$ and $g = 1$, (6) is known as Chan-Vese model [6].

For the piecewise constant model, the contour evolution rule becomes

$$C_t = \sum_{i \in N(x)} \left[(I(x) - c_i)^2 + \frac{\mu}{2}\left(\kappa_i g - \langle \nabla g, \mathbf{n}_i \rangle\right) \right] \mathbf{n}_i. \qquad (7)$$

For a given contour C, the optimal distribution parameters are obtained according (4), by least squares minimization

$$c_i^* = \frac{\int_{\Omega_i} I(x) dx}{\int_{\Omega_i} dx}. \qquad (8)$$

General intensity distribution model In most natural scenarios, image intensity values in regions Ω_i cannot be modelled by a single Gaussian distribution, as in

the piecewise constant model above. To address a broader class of images in our segmentation framework, we can model the intensity distribution in each region using, for example, kernel density estimation [52], [53], Gaussian mixture model [54], *etc*. Here, we estimated these discrete densities using sums of Dirac delta distributions, as follows

$$P(z|\alpha_i) = \frac{1}{|\Omega_i|} \sum_{x \in \Omega_i} \delta_{z=I(x)}, \ z \in [0,1]^d, \qquad (9)$$

where $d = 1$ for grayscale images and $d = 3$ for images given in RGB or CIE-Lab color spaces. Specifically, we found that modelling image intensities using 32^d intensity histograms produced satisfactory segmentation results, as shown in Sect. 5.

Gaussian mixture model The Gaussian mixture model can be integrated into our framework, to model the intensity value distributions, as follows. In that setting, the intensity probability distribution in region Ω_i is given by a weighted sum of K Gaussians

$$P(z|\alpha_i) = \sum_{j=1}^{K} \lambda_i^{(j)} \mathcal{N} \left(z \mid c_i^{(j)}, \sigma_i^{(j)} \right), \qquad (10)$$

where $\mathcal{N} \left(z \mid c_i^{(j)}, \sigma_i^{(j)} \right)$ is the jth component of the Gaussian mixture in the region Ω_i, with mean $c_i^{(j)}$ and covariance matrix $\sigma_i^{(j)} I$. Different components are mixed with weights $\lambda_i^{(j)}$, such that $\sum_{j=1}^{K} \lambda_i^{(j)} = 1$. In this case, the curve evolution rule is obtained by substituting the probability density in Eq. (5) with the Gaussian mixture above.

The optimal model parameters α_i^*, where

$$\alpha_i = \left\{ \lambda_i^{(j)}, c_i^{(j)}, \sigma_i^{(j)} \right\}_{j=1}^{K}, \qquad (11)$$

are calculated as suggested in Eq. (4), using the Expectation Maximization (EM) algorithm [54].

Finally, note that though the above problem formulations are given in terms of the image intensity values, different image representations, for instance, Gabor filter responses or textons for texture segmentation, can be easily utilized in the suggested framework.

2.3 Pairwise dissimilarity model

Pairwise dissimilarity models were previously suggested in [49], [46], [47]. For two-region segmentation problem, with $\Omega = \Omega_{in} \cup \Omega_{out}$, the energy functional data is given by

$$E_{data}(C) = \iint_{\Omega_{in} \times \Omega_{in}} w(x,y)dxdy$$
$$+ \iint_{\Omega_{out} \times \Omega_{out}} w(x,y)dxdy, \qquad (12)$$

where $w(x_1, x_2)$ is the measure of dissimilarity between pixels x_1 and x_2 in Ω_{in} or in Ω_{out}. The two terms of the above model measure the total dissimilarity of the image inside the two regions Ω_{in} and Ω_{out}.

Extension of the above model for the multi-region case is straightforward

$$E_{data}(C) = \sum_i \iint_{\Omega_i \times \Omega_i} w(x,y)dxdy, \qquad (13)$$

where as before $\Omega = \{\cup_i \Omega_i\}$ [46], [47].

Proposition 2.1: Steepest descent step minimizing the data term $E_{data}(C)$ in Eq. (13) is given by

$$C_t = - \sum_{i \in N(C)} \left[\int_{\Omega_i} (w(y,x) + w(x,y)) \, dy \right] \mathbf{n}_i, \quad (14)$$

where $x \in C$, and $\mathbf{n}_i$ is the normal to C at x.
The proof of the proposition is given in Appendix A.

The regularized contour evolution equation for the pairwise dissimilarity model is then given by

$$C_t = \sum_{i \in N(x)} \left[\int_{\Omega_i} (w(y,x) + w(x,y)) \, dy \right.$$
$$\left. + \frac{\mu}{2} \left(\kappa_i g - \langle \nabla g, \mathbf{n}_i \rangle \right) \right] \mathbf{n}_i. \qquad (15)$$

2.4 Pairwise dissimilarity model: examples

We tested the proposed approach with two dissimilarity models suggested in [46] and [47]. The former model measures pairwise pixel dissimilarity by comparing the corresponding image values, in CIE-Lab color space, as follows

$$w(x,y) = \left\| I^{Lab}(x) - I^{Lab}(y) \right\|_2$$
$$= \left(\sum_{l=L,a,b} (l(x) - l(y))^2 \right)^{\frac{1}{2}}. \qquad (16)$$

In the latter paper [47], the authors used a patch-based pixel dissimilarity measure. Define a patch of size $r \times r$ centred at a pixel $x \in \Omega$ by

$$p_x(v) = I(x+v), \quad \forall v \in [-r/2, r/2]^2. \qquad (17)$$

Then, the patch-based pairwise pixel dissimilarity is given by

$$w(x,y) = G_\sigma(x,y)d_p(p_x, p_y), \qquad (18)$$

where $d_p(p_x, p_y)$ denotes a distance measure between two patches p_x and p_y. This patch distance may be defined, for instance, as

$$d_p(p_x, p_y) = \int G_a(v)\|p_x(v) - p_y(v)\|^2 dv. \qquad (19)$$

3 LEVEL SET FRAMEWORK

According to the active contours model, the contour evolution rule, obtained using the first variation of the energy functional $E(C)$ with respect to C, is

$$C_t = -\frac{\delta E(C)}{\delta C} = F\mathbf{n}, \qquad (20)$$

where F denotes the evolution force applied to the evolving contour in the normal direction $\mathbf{n}$.

The contour evolution can be re-formulated ([2], [34], [4], [6]) in the level set framework of [33]. A level set function $\phi(x)$ is defined such that the contour C is given by its zero level set

$$C = \{x \mid \phi(x) = 0\}, \qquad (21)$$

ϕ is negative inside the region defined by C, and positive outside. Note that C consists of one or more simple, possibly closed, curves, each of which can be parameterized as a mapping from $\mathbb{R}$ to $\mathbb{R}^2$. Thus, except for the junction points, this definition of C is consistent with the definition as a mapping from $\mathbb{R}$ to $\mathbb{R}^2$, given at the beginning of Section 2.

As was shown in [33], evolving the curve according to Eq. (20) is equivalent to evolving the level set function according to

$$\phi_t = F_{ext} \left| \nabla \phi \right|, \qquad (22)$$

where F_{ext} is a smooth extension of the force F to the entire domain Ω, or, alternatively, to a narrow band around the evolving contour [55], and subject to $F_{ext}(C) = F$. For efficient techniques for constructing extension velocities see [56].

This conventional framework is well suited for two-region segmentation, where C divides the image into an object and a background, but it cannot be trivially extended for multi-region segmentation. Previous methods for multi-region segmentation, based on the level set framework, require either managing multiple level set functions to execute the multi-region active contour evolution [36], [38], [41], or exploit level functions specifically designed to describe multiple evolving regions [16], [43].

Here, we present a new method for multi-region active contour evolution, using a single level set function and exploiting the Voronoi Implicit Interface Method [44], [45], [48], that we describe in the next section.

3.1 Description of the Voronoi Implicit Interface Method

The Voronoi Implicit Interface Method (VIIM) [44] was recently introduced for numerical solution of interface propagation problems with arbitrary number of phases (regions), arising in the area of computational fluid dynamics. In 2D, the interface between the phases is a set of 1D curve segments, meeting at

tripple-junctions. Figure 2(a) demonstrates an example of such an interface (the black solid curve), with two triple-junctions with different intersection angles. In 3D the interface is given by a set of 2D surface segments.

The interface propagation is governed by the equation $C_t = F\mathbf{n}$. A single non-negative level set function $\phi(x), x \in \mathbb{R}^d$ is used to evolve C. This function is given by an *unsigned* distance from the interface C. Hence, the interface C is the zero level set of the function $\phi(x)$, similar to the conventional level set framework

$$C = \{x \mid \phi(x) = 0\}.$$

The level set function evolution is again governed by the equation

$$\phi_t = F_{ext} \left| \nabla \phi \right|, \qquad (23)$$

where F_{ext} is the extension velocity, mentioned in the previous section. Examples given in [44] include curvature and mean curvature flows, as well as physical simulations of the dynamics of dry foams.

For some small ε, observe the evolution of the ε-level sets of ϕ

$$C_\varepsilon = \left\{x \in \mathbb{R}^2 \mid \phi(x) = \varepsilon\right\}. \qquad (24)$$

According to the comparison theorem, two evolving ε-level sets will always encapsulate the evolving zero level set they are adjacent to [44]. Moreover, these ε-level sets of ϕ are necessarily simple curves. Thus, their evolution is well defined in terms of the conventional level set framework. The main observation of [44] consists in the following: the evolving ε-level sets of the function ϕ can be used to reconstruct the evolving interface, which is assumed to lie at an equal distance from the two ε-level sets adjacent to it. Thus, the interface may be reconstructed from these new ε-level sets C_ε as follows.

1) Compute Voronoi regions of difference segments of C_ε in the narrow band $\{x|\phi(x) < \varepsilon\}$.
2) Reconstruct the interface C from intersections of these Voronoi regions.

In order to evolve the interface as described above, the following three step-algorithm was suggested in [44].

1) Evolve the level set function ϕ according to Eq. (23), using a small time step dt.
2) Find the ε-level sets of the new function, and reconstruct the interface C, as described above. Update the level set function ϕ using the reconstructed interface.
3) Update the propagation speed function F; return to Step 1.

Figure 2 illustrates different steps of the algorithms and the contour obtained after one algorithm iteration. We note that step 2 of the algorithm constrains the regions $\{\Omega_i\}_{i=1}^M$ so as to form a partition of the domain, as is expected in segmentation models such as the region competition model.
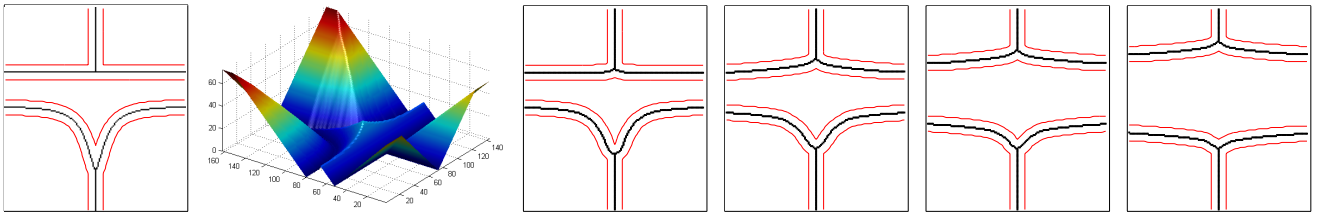
Fig. 2. The VIIM contour evolution illustration, with Neumann boundary conditions. Left to right: original contour C (shown in black) with ε-level sets (show in red); corresponding level set function $\phi(x,y)$; ε-level sets of $\phi(x,y)$ and the evolved contour, at different stages of the evolution.

4 MULTI-REGION ACTIVE CONTOURS: THE PROPOSED APPROACH

We propose to adapt the Voronoi Implicit Interface Method, described above, to solve the multi-region segmentation problem that was defined in Sect. 2. The VIIM was formulated in terms of a general interface velocity F; thus, it is applicable to various interface evolution problems which may be solved using the level set approach. Specifically, the contour evolution rule for both the region competition and the pairwise dissimilarity models, discussed in Sect. (2), can be written as

$$C_t = \sum_{i \in N(x)} \left[F_i(x) + \frac{\mu}{2} F_i^{gac}(x) \right] \mathbf{n}_i. \qquad (25)$$

The force F_i in the above equation depends on the chosen model: for the region competition model it is

$$F_i(x) = -\log P\left(I(x)|\alpha_i\right), \qquad x \in C, \qquad (26)$$

and for the pairwise dissimilarity model the force is

$$F_i(x) = \int_{\Omega_i} \left(w(y,x) + w(x,y)\right) dy, \qquad x \in C. \qquad (27)$$

The regularizing geodesic active contours force $F_i^{gac}(x)$ is given by

$$F_i^{gac}(x) = \kappa_i g - \langle \nabla g, \mathbf{n}_i \rangle, \qquad x \in C. \qquad (28)$$

To use the level set formulation, the contour velocity has to be extended to the entire domain Ω (or to a narrow band around the evolving interface) to obtain $F_{ext}(x)$. Given this extension velocity, the level set function is evolved according to the evolution rule in Eq. (23). Extension of the regularization velocity to the entire domain Ω is performed, for example, using the standard definition of [4]

$$F_{ext}^{gac}(x) = \text{div}\left(g(x)\frac{\nabla \phi}{|\nabla \phi|}\right). \qquad (29)$$

The suggested construction of the extension velocity for the term $\sum_i F_i(C)\mathbf{n}_i$ is described in the following section.

4.1 Extension velocity construction

Let us define by C_{ij} a part of the contour C separating two regions Ω_i and Ω_j. For each point $x \in \Omega$, identify the part of the contour C_{ij} closest to x, as follows

$$d\left(x, C_{ij}\right) < d\left(x, C_{kl}\right), \qquad \forall k, l, \qquad (30)$$

where

$$d\left(x, C_{ik}\right) = \min_{y \in C_{ik}} \|x - y\| \qquad (31)$$

is the minimal Euclidean distance between the point x and any $y \in C_{ik}$. Such a point x necessarily belongs to either Ω_i or Ω_j. Following the notations used in [44], [45], we denote the set of all points $(x,y) \in \Omega$ satisfying Eq. (30) by the *Voronoi region* of the segment C_{ij}, $\text{Vor}(C_{ij})$.

Using the above definition, the extension velocity at $x \in \Omega_i$ reads

$$F_{ext}(x) = F_i(x) - F_j(x), \qquad x \in \text{Vor}(C_{ij}). \qquad (32)$$

Notice that for the two-region case, the above extension velocity produces the conventional evolution rule, suggested, for instance, in [6] and in [49], up to a sign change that follows from the fact that our level set function is non-negative everywhere in the domain Ω.

Note that in a previous paper [48], we suggested to define this extension velocity by

$$F_{ext}(x) = F_i(x), \quad x \in \Omega_i. \qquad (33)$$

According to it, the level set function evolution in each region Ω_i depends on the statistics of this region alone. In addition, $F_{ext}(x)$ defined as above, is smooth within every region Ω_i. The straightforward extension of the contour velocity suggested in Eq. (32) may, theoretically, produce velocity profile with discontinuities at the boundaries of the Voronoi regions of different contour segments. However, in practice this new definition of extension velocity produces more accurate region boundaries than the previous one (33), as illustrated by the segmentation results shown in Figure 3.

Original image   Final contour   Mean intensity values   Close-up view of the obtained contour
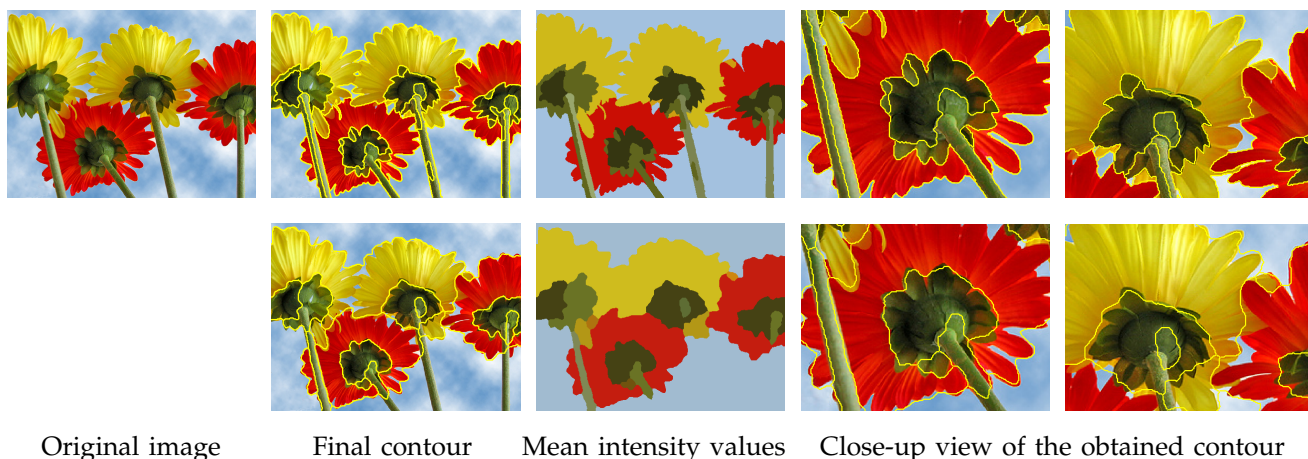
Fig. 3. Comparison of results produces using the proposed method with two extension velocities F_{ext} described in Sect. 4. Upper row: the original image (left), results obtained using the extension velocity suggested in this paper. Bottom row: results obtained using the extension velocity suggested in [48].

Finally, to obtain the evolution rule for the level set function $\phi(x)$ we combine Eq. (29) and Eq. (32)

$$\phi_t(x) = \left[F_i(x) - F_j(x) + \mu \text{div}\left(g(x)\frac{\nabla\phi}{|\nabla\phi|} \right) \right]|\nabla\phi|,$$
$$\text{for } x \in \{\Omega_i \cap \text{Vor}(C_{ij})\}. \quad (34)$$

With the above level set function evolution rule, the proposed algorithm for multi-region segmentation reads as follows. Define some initial contour $C = C_0$, and compute its corresponding unsigned distance level set function $\phi(x)$. Repeat the following steps, until convergence.

1) Compute the extension velocity in each region Ω_i, and evolve the level set function $\phi(x)$ according to the evolution equation (34).
2) Extract the ε-level sets of the evolved level set function. Extract the Voronoi regions of these ε-level sets in the narrow band $\{x : \phi(x) < \varepsilon\}$, and reconstruct the evolved contour C as the collection of the boundaries between these Voronoi regions.
3) Perform re-distancing: re-calculate the unsigned level set function $\phi(x)$ using the new contour C. Return to Step 1.

4.2 Volumetric image segmentation

The above formulation can be easily extended to segment volumetric data, such as video, medical volumetric data (CT or MRI scans), *etc*. As in the two-dimensional case, the segmentation problem is formulated as a minimization of the energy functional

$$E(S) = E_{data}(S) + \mu E_{reg}(S), \quad (35)$$

where S is the set of intersecting two-dimensional surface segments, defining boundaries of three-dimensional regions. Different image appearance models, discussed in Sect. 2.2, can be applied for

volume segmentation as is. The regularization energy term is now given by

$$E_{reg}(S) = \frac{1}{2}\sum_i \oint_{S_i} g(S_i(u,v))da(u,v), \quad (36)$$

where $S_i(u,v) : \mathbb{R}^2 \to \mathbb{R}^3$ is a parameterized two-dimensional surface describing the boundary of the region $\Omega_i \in \Omega$, and $da(u,v) = |S_u \times S_v|dudv$ is an area element at the point $S_i(u,v)$ [35], [50]. For instance, the 3D region competition model reads

$$E(S, \{\alpha_i\}) = \sum_i \int_{\Omega_i} -\log P(I(x)|\alpha_i)\, dx$$
$$+ \frac{\mu}{2}\sum_i \oint_{S_i} g(S_i(u,v))da(u,v), \quad (37)$$

where $I(x)$ is now a volumetric image, defined on the domain $\Omega \subset \mathbb{R}^3$.

Here as well, we use the level set formulation to evolve the surface towards minimum of $E(S)$ above. The surface S is represented implicitly as the zero level set of the level set function $\phi : \mathbb{R}^3 \to \{\mathbb{R}^+ \cup 0\}$,

$$S = \{x \in \mathbb{R}^3 \mid \phi(x) = 0\}. \quad (38)$$

The level set function evolution is performed using the suggested multi-region framework, according to the evolution rule in Eq. (34), where the forces $F_i, \forall i$, are calculated as described in Eq. (26) or Eq. (27).

4.3 Implementation considerations

The level set function evolution is performed on a fixed grid of size h, in 2D or 3D. In all our experiments, the narrow band level set evolution technique of [55] was used to reduce the computation complexity. Both ε-level set extraction and level set function re-initialization were performed with subpixel precision, to obtain an accurate contour. The level set function was re-initialized after each evolution step. Following

[45], we set ε to be an integer multiple of the grid size h, to ensure numerical convergence of the proposed method. In our experiments, we used $h = 1$ and $\varepsilon = 3h$.

Algorithm intialization In our experiments, we used two types of initial contours. For the first, we used multiple equally spaced circles, or rectangular grid boundaries, defining the initial regions (see Figure 9). For the second, the initial regions were obtained using k-means or mean shift clustering. Note that the latter initialization is naturally suited for the piecewise constant segmentation model.

Discrete level set function evolution When using the explicit forward time derivative to perform the level set function evolution according to Eq. (34), the geodesic active contour term imposes a constraint on the time step required for stability. In our implementation, we combined an explicit forward time derivative to perform the evolution according to the velocity derived from the data term, with the unconditionally stable semi-implicit LOD scheme [57], to perform the geodesic active contour evolution, similar to [51].

Contour reconstruction from the ε-level sets Let us denote by C_ε^i the ε-level set of the evolved function $\phi(x)$ in the region Ω_i. The new contour C is reconstructed by taking all points in the region $\{x \in \Omega \,|\, \phi(x) < \varepsilon\}$, that are equidistant from a pair of their closest ε-level sets

$$C = \{ \, x \mid \mathrm{d}(x, C_\varepsilon^i) = \mathrm{d}(x, C_\varepsilon^j) \leq \mathrm{d}(x, C_\varepsilon^k),$$
$$\text{for some } i, j, \text{ and any } k \neq i, j \, \}. \quad (39)$$

The distances $\mathrm{d}(x, C_\varepsilon^i)$ are computed for each level set C_ε^i and the image pixels in the region $\{x \in \Omega \,|\, \phi(x) < \varepsilon\}$ using the fast marching method of [58].

Finally, we recompute the unsigned distance from the new contour C, using the fast marching method. To compute the distances with subpixel precision, one may initialize the fast marching method using the distances $\mathrm{d}(x, C_\varepsilon^i)$ computed at the previous step, and the re-initilaization technique described in [59], or calculate the distances to the new contour explicitly [51]. In our experiments, explicit contour extraction was performed only to visualize boundaries of the obtained regions.

Region creation and destruction In the course of the level set function evolution, regions may be created, or may disappear as a consequence of the regularization. However, the proposed framework does not allow two adjacent regions to merge. To overcome a similar problem, in [8] the authors suggested to merge pairs of adjacent regions, if the merging decreased the energy functional. In our experiments, we adopted this approach and performed region merging after each redistancing step.

However, evaluating the above test for every pair of adjacent regions at each algorithm iteration may be computationally demanding. Alternatively, region merging can be performed using the following simple heuristic approach: two regions Ω_i and Ω_j are merged if they have sufficiently similar intensity statistics. For the piecewise constant model, regions Ω_i and Ω_j are merged when their corresponding mean intensity values c_i and c_j are closer than some predefined threshold T_c

$$\|c_i - c_j\|_2 \leq T_c. \quad (40)$$

In the case of the general region competition model, image intensity values in regions Ω_i are described by probability density functions $p_i(z) = p(z|\Omega_i)$. The merging criterion can be based on the dissimilarity between pairs of probability density functions, and measured using the χ-squared distance, for instance,

$$d(p_i, p_j) = \frac{1}{2} \frac{\sum_z (p_i(z) - p_j(z))^2}{\sum_z p_i(z) + \sum_z p_j(z)} \leq T_p. \quad (41)$$

Other distance measures between distributions may be used as well.

The two above criterions are well suited for applications where the required region similarity is known in advance. In more complex scenarios, the energy minimization criterion may be applied. Since there is no equivalent simple region similarity criterion for the pairwise dissimilarity models, for these models the energy minimization or the heuristic merging criterion given in Eq. (40) can be used.

We note that a more general model is one where the number of regions is unbounded. For this model, other region merging and also splitting methods can be used to define additional, non-local, optimization steps. We leave the discussion of alternative split and merge steps in our model for future work.

Algorithm complexity In terms of memory consumption, the proposed method requires additional space of order of the number of image pixels. The computational complexity of the proposed approach is determined by the redistancing, extension velocity computation and region merging steps. Let us denote by n the number of pixels in the narrow band around the evolving contour, and by m the number of different image regions detected at some algorithm iteration. During the redistancing step, the new contour can be obtained from ε-level sets in $O(n \log n)$ time, and the distance function can be recomputed in $O(n \log n)$ time, using the fast marching method. Thus, the total complexity of the redistancing step is $O(n \log n)$.

The following components of the computation time depend on the chosen model: the model parameter update time, required for the region competition model, the extension velocity computation, and region merging. The model parameter update step, for the piecewise constant case, or for the general intensity distribution modelled using KDE, can be performed incrementally, using only the pixels inside the Voronoi regions of ε-level sets. For the Gaussian mixture

model, the update step requires computation over the entire image domain.

The extension velocity F_{ext} computation time, in the simplest case of the piecewise linear model, is linear in the number of the narrow band pixels, n, while for the more complex pairwise dissimilarity model, computation over the entire image domain may be required. Note that this and the previous computation time components are not specific to the proposed method alone, since similar computation would be required by any algorithm minimizing the energy functionals (3) and (13), discussed in Section 2.

Region merging based on energy minimization can be computationally demanding, and in general may require multiple computations over the detected image regions, after each algorithm iteration. When using the region competition model, the heuristic region merging may be applied alternatively, to facilitate the computation. It requires calculating $m(m-1)/2$ dissimilarity values, according to Eq. (40), which may be performed in $O(m^2)$ time, or Eq. (41), for which the required number of operations is m^2 multiplied by the time it takes to evaluate a single pdf. This brute-force implementation can be further improved by merging only pairs of neighbouring regions, which can be preformed in $O(m)$ rather than $O(m^2)$ time. Note that here we assume that $m \ll |\Omega|$ (the number of image pixels), which makes this merging procedure very efficient.

5 RESULTS AND DISCUSSION

In this section we present the segmentation results obtained using the proposed method, combined with different data energy terms described above. In most of our experiments we used the natural images from the Berkeley Segmentation Dataset (BSDS500) [25]. The proposed method was applied to color images, in RGB or CIELAB colorspaces, with intensity values normalized to the range $[0, 1]$.

5.1 Image segmentation

Figure 4 presents a comparison of the proposed method, the convex relaxation method of Chambolle and Pock [19], and the graph-cut based approach of [15]. The proposed method was applied with the piecewise constant region competition model described in Section 2.2, Eq. (6). [19] minimizes the same energy functional, up to the regularization term, which is given by the total contour length, while [15] minimizes its discrete counterpart with an additional label cost term. To make the proposed method and [15] comparable in terms of the minimized energy functional, we set the weight of this additional term to zero, effectively obtaining the algorithm described in [13]. Figure 5 presents the results obtained using the proposed method and the algorithm of [19], together with the manual "groundtruth" segmentation

provided for the BSDS500 [25]. For both [19] and [15], we used the implementation provided by the authors, and optimized the algorithm parameters to obtain visually optimal results. The proposed method was initalized using k-means clustering, and the algorithm parameters were kept constant for the three images. From examining the images in Figures 4 and 5, we observe that the three methods indeed produce comparable results.

Figure 7 presents segmentation results, obtained for images from the BSDS500 using the proposed method with the region competition model. The proposed method was applied with two variants of the region competition model, that were described in Sect. 2.2, and with the two region merging algorithms described in the previous section. When applied with the heuristic region merging algorithm, with relatively low region similarity thresholds, the proposed method produces very detailed segmentation results - see the 2nd and the 4th columns in Figure 7. The level of details in the obtained segmentation can be further adjusted by varying the region similarity thresholds T_c and T_p. When applied with region merging based on energy minimization, our method produces results that are less fragmented, and more similar to manual semantic region labelling - see the 3rd and the 5th columns in Figure 7.

Figure 8 presents more results obtained for images from the BSDS500 using the proposed method, alongside results obtained with [19] and [15]. The proposed method was applied in both RGB and CIELAB colorspaces, using the same set of parameters; [19], [15] were applied in RGB colorspace, where they obtained visually optimal results. For the proposed method to be able to detect thin image regions, such as the wickerwork in the upper example, the images were scaled to be twice their original size, that is 642×962 or 962×642 pixels, prior to the segmentation.

For the three images presented in Figure 8, we also examined the computation time of the proposed method, and compared it to [19], [15]. The proposed method, [15] and [19] were terminated after $50, 20$ and 250 iterations, respectively (chosen so that all the algorithms would produce similar segmentation results), or when less than 0.01% of all image pixels were assigned new labels at a certain iteration. All three implementations took several minutes on a laptop with an Intel Core i7 processor and 16 GB RAM. The proposed method, applied with the piecewise constant model and heuristic region merging, was slightly faster than [19]. [15] showed best performance in terms of computation time, terminating after a couple of minutes, at the cost of some visible metrication errors, which can be noticed in Figure 8(f). It is important to note that the proposed algorithm was implemented in Matlab, without performance considerations in mind, while [15] is a C based efficient implementation. For [19], a Matlab implementation

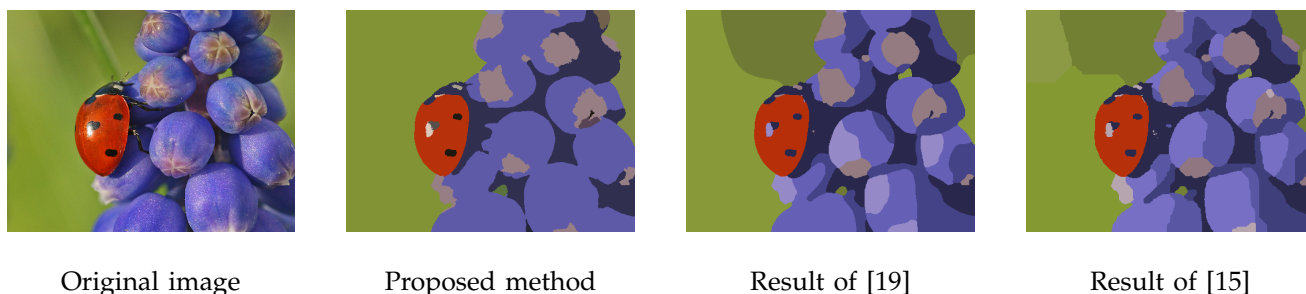| Original image | Proposed method | Result of [19] | Result of [15] |

Fig. 4. Segmentation result obtained with the proposed method, applied with the piecewise constant model, and the results obtained with the algorithms of Chambolle and Pock [19] and Delong *et al*. [15].
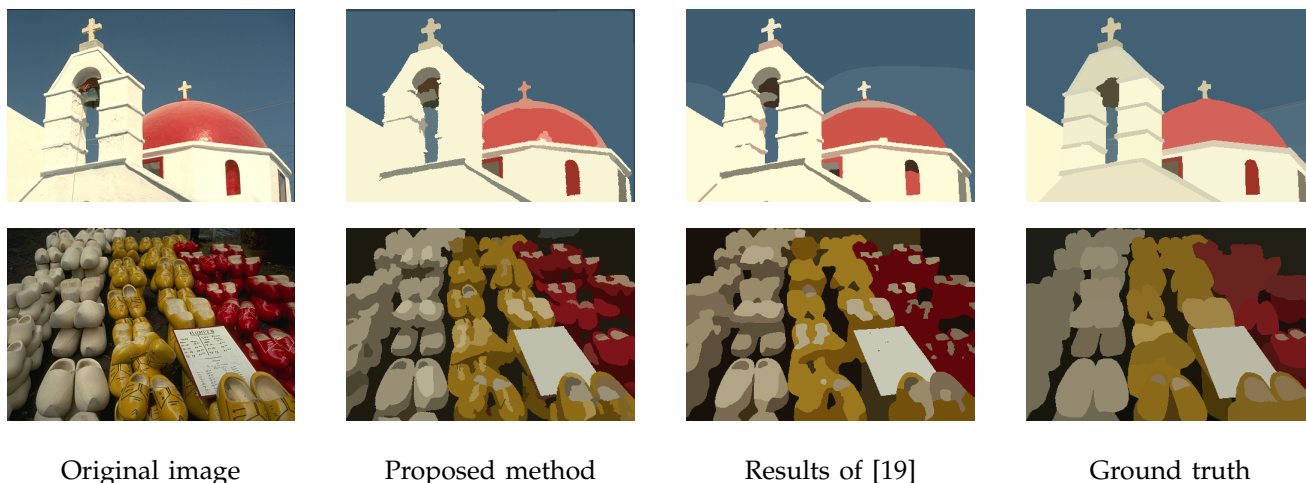

| Original image | Proposed method | Results of [19] | Ground truth |

Fig. 5. Comparison of the results obtained with the proposed method, applied with the piecewise constant model, the method of Chambolle and Pock [19], and the manual "ground truth" segmentation [25].

provided by the authors was used. Applying the proposed method with the general region competition model increases the computation time of the proposed method, in accordance with the algorithm complexity analysis presented above.

To perform quantitative evaluation of the proposed method, we used the evaluation framework suggested in [24], [25]. According to it, the detected regions boundaries are compared to several manual segmentations given for every image, producing a precision-recall segmentation score. An F-measure is then calculated as $\left(\frac{2 \cdot Precision \cdot Recall}{Precision + Recall} \right)$. Higher F-measure corresponds to better agreement with manual segmentations. The region detection quality was evaluated using the variation of information, the rand index, and segmentation covering measures - for a detailed description of each of these measures see [25].

Figure 6 presents a plot of the F-measure values obtained using the proposed method with the piecewise constant model for the test images from the BSDS500. Different $Precision - Recall$ pairs were obtained by varying the weight of the regularization term μ. Additional results shown in Figure 6 correspond to the boundary detection algorithm of [25], and additional segmentation methods discussed therein.

Tables 1 and 2 present region and boundary benchmarks on the BSDS500. The learning approach of Arbelaez *et al*. [25], whose parameters were optimized over the training images from the BSDS500, and the new spectral clustering method utilising multi-layer affinities of Kim *et al*. [26], perform best among all the compared methods. The proposed method, while not as accurate as [25], [26], outperforms most of other segmentation methods, including the mean shift and the multiscale normalized cuts algorithms of [21], [22], in terms of the F-measure. This is despite the fact that it was applied using the very simple assumption of piecewise intensity constancy in image regions.

Figure 9 presents the segmentation results obtained using the proposed method for various initial contours. For comparison, it also presents the results obtained with [15] and [19], for some of the examined contours. Both [15] and [19] were initialized using the number of the regions defined by the initial contours, and mean intensity values in these regions, and applied in the RGB colorspace, where they produced optimal results. While the results of the proposed method clearly depend on the initialization, our algorithm produces reasonable segmentation results for most types of initial contours. Note that [15], [19] produce segmentation with the number of regions
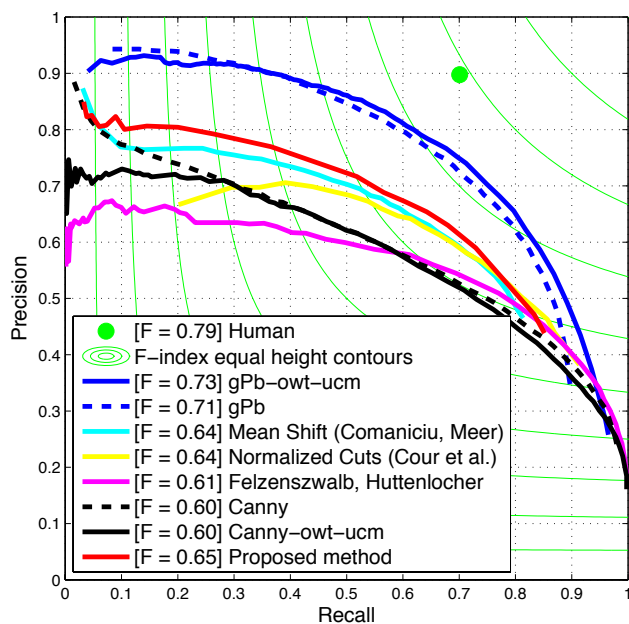
Fig. 6. Boundary benchmarks on the BSDS500: precision-recall plots and the best F-measures obtained for different algorithms.

	ODS	OIS	AP
Our method	0.65	0.68	0.51
gPb-owt-ucm [25]	0.73	0.76	0.73
gPb [25]	0.71	0.74	0.65
Canny	0.60	0.63	0.58
Mean Shift [21]	0.64	0.68	0.56
NCuts [22]	0.64	0.68	0.45
Canny-owt-ucm [25]	0.60	0.64	0.58
Felz-Hutt [23]	0.61	0.64	0.56
FNCut [26]	0.67	0.71	0.44
fPb-owt-ucm [26]	0.69	0.71	0.62
cPb-owt-ucm [26]	0.72	0.75	0.73

TABLE 1
Boundary benchmarks on BSDS500. Shown are F-measures obtained with a single optimal parameter selection for all test images (ODS), optimal parameter selection per image (OIS), and the average precision (AP). Results in the upper row correspond to the proposed method.

	Covering			PRI		VI	
	ODS	OIS	Best	ODS	OIS	ODS	OIS
Our method	0.54	0.60	0.70	0.79	0.83	1.89	1.64
gPb-owt-ucm	0.59	0.65	0.74	0.83	0.86	1.69	1.48
Canny-owt-ucm	0.49	0.55	0.66	0.79	0.83	2.19	1.89
Mean Shift [21]	0.54	0.58	0.66	0.79	0.81	1.85	1.64
Felz-Hutt [23]	0.52	0.57	0.69	0.80	0.82	2.21	1.87
NCuts [22]	0.45	0.53	0.67	0.78	0.80	2.23	1.89
FNCut	0.53	0.60	-	0.81	0.84	1.86	1.59
fPb-owt-ucm	0.58	0.63	-	0.82	0.85	1.70	1.50
cPb-owt-ucm	0.59	0.65	-	0.83	0.86	1.65	1.45

TABLE 2
Region benchmarks on BSDS500. Shown are the Best covering (Covering), the Probabilistic Rand Index (PRI), and the Variation of Information (VI) measures, obtained with a single optimal parameter selection for all test images (ODS), optimal parameter selection per image (OIS), and the average precision (AP). Results in the upper row correspond to the proposed method. The results *gPb-owt-ucm* and *Canny-owt-ucm* correspond to [25], and *FNCut, fPb-owt-ucm, cPb-owt-ucm* - to [26].

equal (or smaller, in case of [15]) to the number of the initial regions. Thus, for too small or too large number of initial contours, [15], [19] may produce sub-optimal results, as can be observed in Figure 9 (g-l).

Figure 10 presents a comparison of the proposed method, and the algorithm of Bertelli et al. [46]. Note that [46] employ a preprocessing step, during which the images are divided into superpixels, which are then used to construct the final segmentation. Thus, the quality of the final region boundaries, produced by [46], strongly depends on the quality the super pixel boundaries. The suggested method was applied with the piecewise constant and the pairwise dissimilarity models. Its segmentation results were comparable, or more detailed than the results presented in [46].

Figure 11 presents a comparison of the proposed method, and the non-local active contours algorithm of [47]. The suggested method was applied with the piecewise constant model, and the pairwise dissimilarity model with the non-local energy measure (18) of [47]. When applied with the piecewise constant model, despite the simplicity of the latter, our algorithm produced accurate segmentation results for both test images, with tighter boundaries, as compared to the results of [47]. When applied with the nonlocal active contour model, our algorithm produced a more fragmented segmentation, due the local similarity measure utilized by this model.

5.2 Volume segmentation

We applied the proposed method to volume segmentation on a simulated brain MRI scan from the BrainWeb dataset[1] [60]. The scan was generated using the following parameters: T1 modality, 1 mm slice thickness, 3% noise, calculated relative to the brightest tissue, and 20% intensity non-uniformity.

Figure 12 presents the segmentation results obtained for a single MRI slice using the piecewise constant segmentation model, and an arbitrarily chosen initial contour, shown in the left image. The algorithm correctly detected the boundaries between the white

1. http://www.bic.mni.mcgill.ca/brainweb/

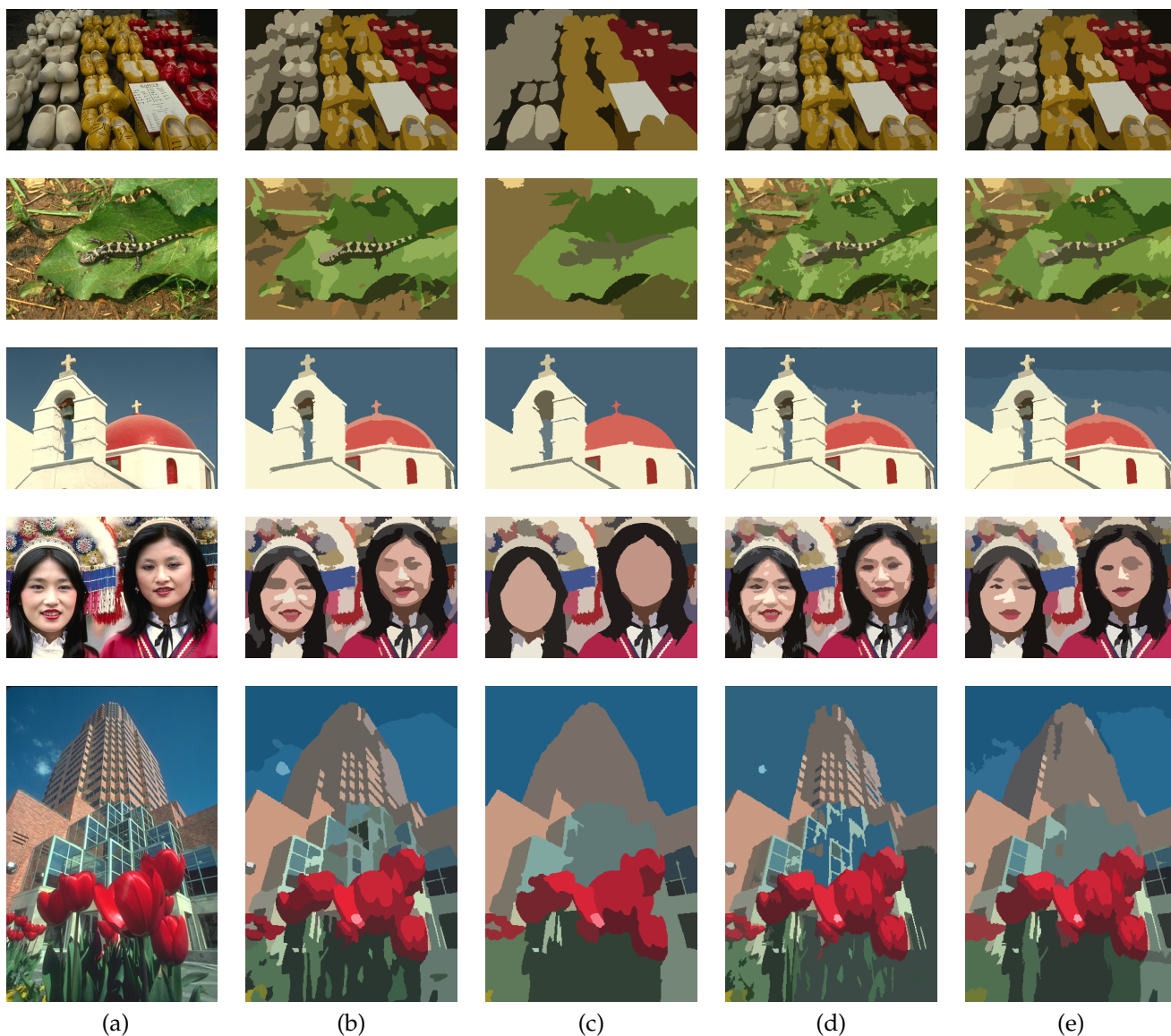| (a) | (b) | (c) | (d) | (e) |

Fig. 7. Segmentation results obtained using the proposed method with piecewise constant and general region competition models. (a) Original image. (b, c) The piecewise constant model, with (b) heuristic region merging with $T_c = 0.05$, and (c) region merging by energy minimization. (d, e) General region competition model, with image intensity pdf modelled by 32^3-bin histogram, (d) heuristic region merging with $T_p = 0.3$, and (e) region merging by energy minimization.

and the gray matter, while missing some of the boundaries between the gray matter and the cerebrospinal fluid (CSF), due to small contrast changes and the fact that the initial contour is located far from these boundaries.

Figure 13 presents the segmentation results obtained using the 3D version of the proposed method, with the piecewise constant segmentation model. The initial segmentation was given by 6 small spheres, arbitrarily placed inside the gray matter outer boundary. Figure 14 presents the comparison of the detected white matter region and the ground truth segmentation. Total of 93.27% of the white matter pixels were correctly classified by our method, producing Dice coefficient $DC = 93.37$ [61]. Mislabeling occurs at the

pixels where there is no significant contrast change between the white matter and the adjacent tissues, and where our algorithm, based on piecewise constant model, is indeed more likely to fail.

We plan to extend the proposed method for color volumetric image and video segmentation. For medical image segmentation, we expect that incorporating prior knowledge about intensity statistics of different tissues will help performing accurate segmentation targeted for more specific tasks, for instance detection of boundaries between pre-specified set of regions. Further evaluation of the proposed method for 3D segmentation, and its application for other types of volumetric data analysis are left for future research.

(a)   (b)   (c)   (d)   (e)   (f)   (g)
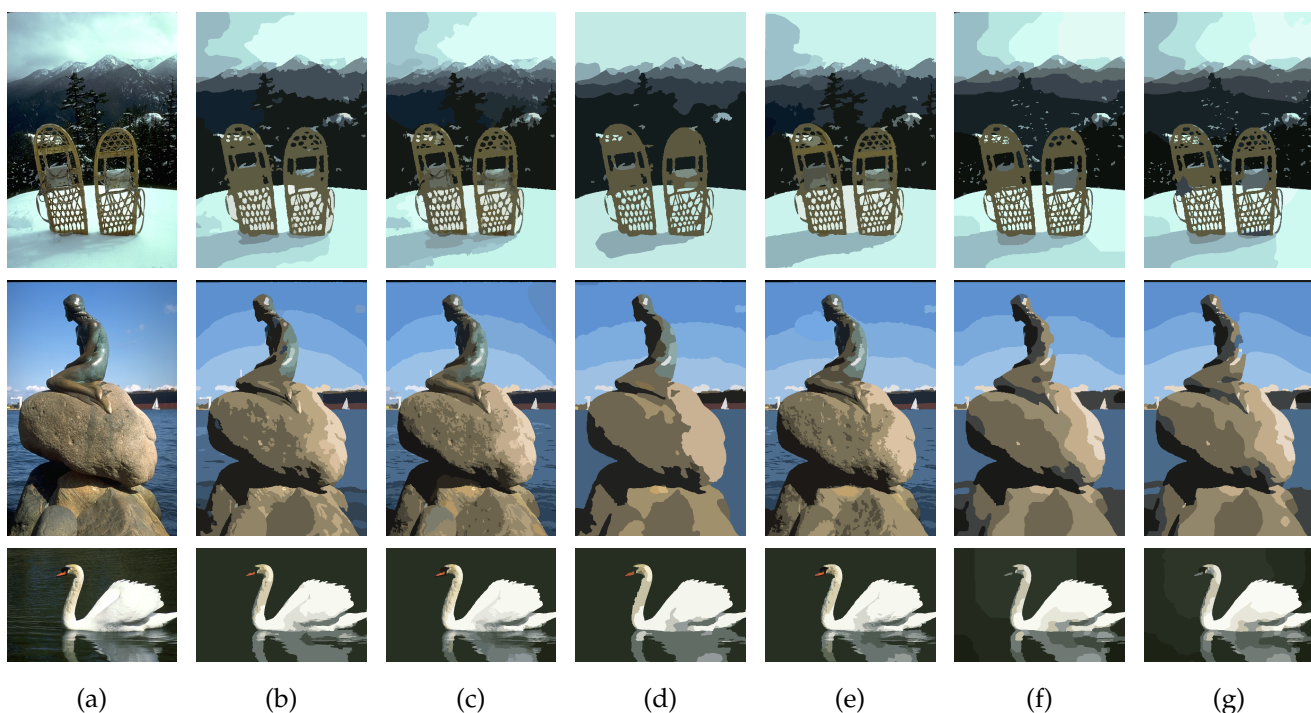
Fig. 8. Additional segmentation results obtained using the proposed method with piecewise constant and general region competition models, using heuristic merging algorithm with $T_c = 0.05$ and $T_c = 0.05$, and results of [15], [19]. (a) Original image; (b, d) piecewise constant model, applied in (b) RGB and (d) CIELAB colorspaces; (c, e) general region competition model, with image intensity pdf modelled using [53], applied in (c) RGB and (e) CIELAB colorspaces; (f) results of [15]; (g) results of [19].

5.3 Algorithm limitations

Initalization and parameter selection As illustrated by Figure 9, the segmentation results are initialization-dependent. Furthermore, parameter tuning may be required to adapt the proposed method to different energy functionals.

Time complexity As mentioned in Section 4.3, calculating the evolution force for the the pairwise model and the region-competition model with general probability density functions is computationally expensive. For the test image presented above, between 50 and 200 iterations were required for convergence. Another time consuming part of the algorithm is region merging based on energy minimization, as opposed to heuristic region merging. According to our experiments, in many cases the region competition model with heuristic region merging is sufficient to obtain good segmentation results, and may be used to facilitate the computation.

5.4 Additional energy models

The proposed method is not limited to the two segmentation models described above. It can be easily extended for texture image segmentation, using the image gradient magnitude, Gabor features, textons, etc., instead of, or in addition to the color features. Our method can also be applied with various edge

alignment functionals, for instance the following functional, suggested in [62], [57], [63],

$$E(C) = \oint_C \langle \nabla I(C(s)), \mathbf{n}(s) \rangle \, ds, \qquad (42)$$

or with a different class of segmentation models for active contours, suggested in [7], [27], [29]. In these papers, the energy functional is designed to measure the discrepancy between empirical distributions of image features inside and outside the segmenting contour. Evaluation and comparison of these and additional multi-region segmentation models will be a subject of future research.

6 CONCLUSIONS

We addressed the problem of segmenting an image into an arbitrary number of regions using a novel multi-region active contours formulation. The proposed framework treats multiple regions in a uniform manner by utilising the new Voronoi implicit interface method, while avoiding metrication errors. It can be applied with various region and boundary appearance priors, for both 2D and volumetric image segmentation, for which it produces accurate and detailed segmentation results.
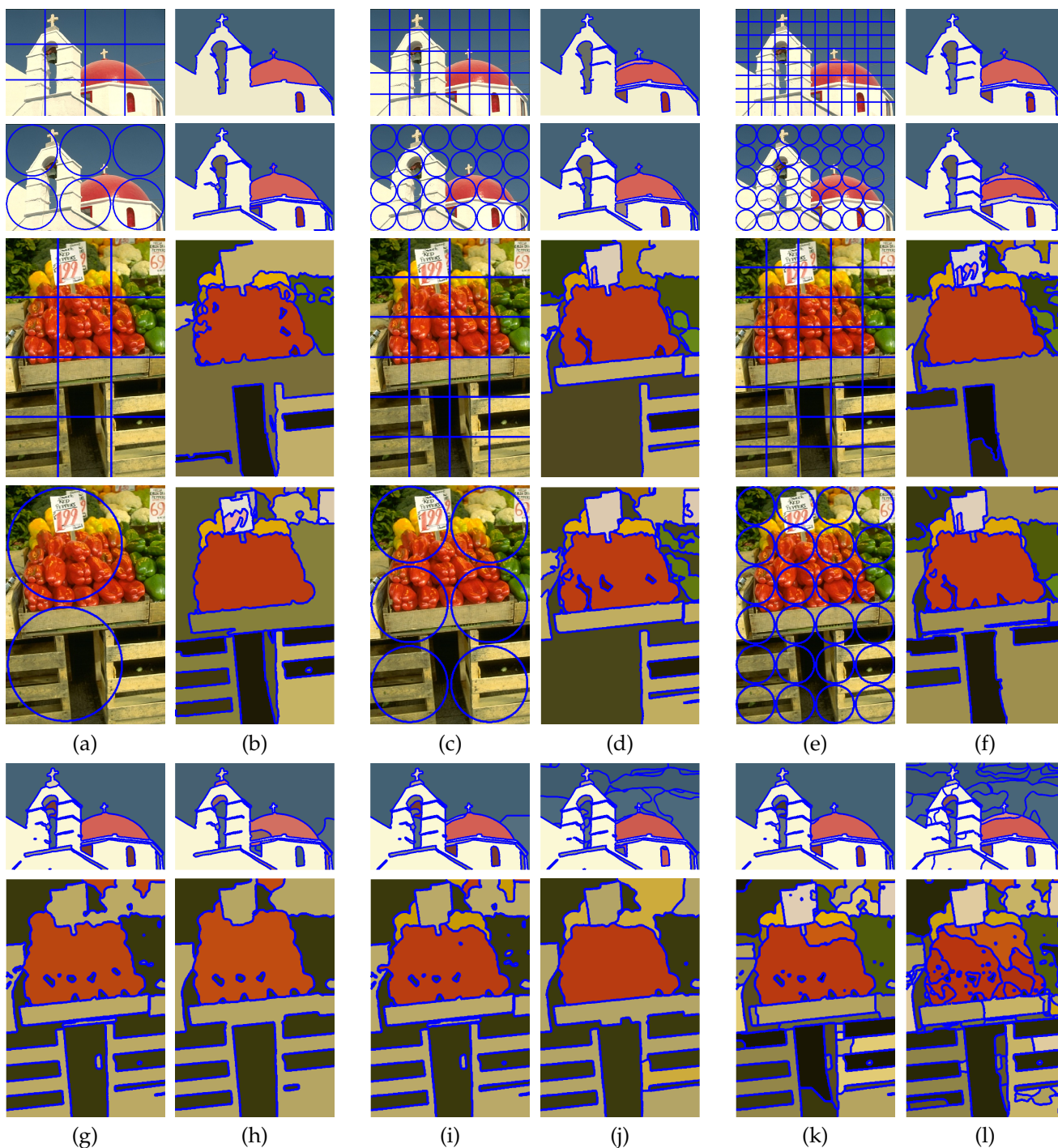
Fig. 9. Segmentation results obtained for various initial contours, with the piecewise constant model and heuristic region merging algorithm. (a, c, e) Initial contours, and (b, d, f) the corresponding segmented images, colored according to mean intensity values in the obtained regions. Results of [15] (g, i, k) and [19] (h, j, l), initialized using the circular initial regions, shown in columns (a, c, e) above, in the second and the fourth rows. See the accompanying text for details.
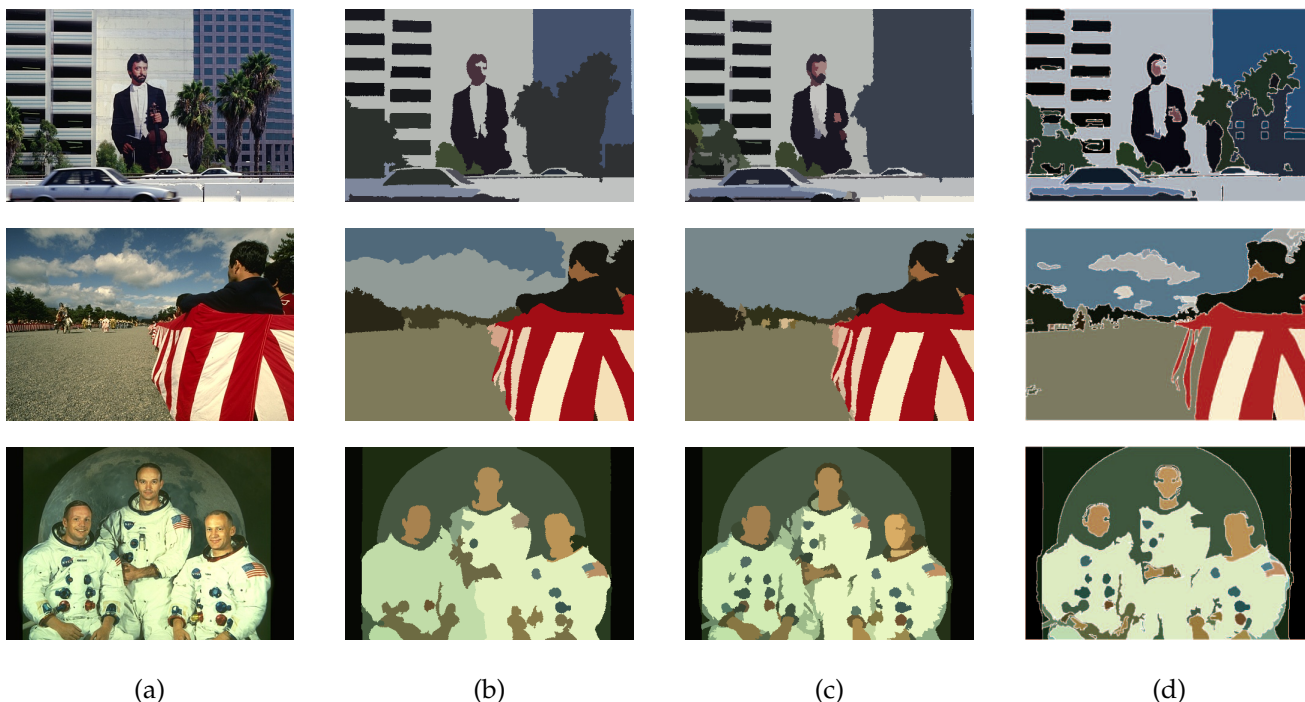
| (a) | (b) | (c) | (d) |

Fig. 10. Comparison of the proposed method and [46]. (a) The original image. (b) Results obtained with our method using the piecewise constant model. (c) Results obtained with our method using the pairwise similarity model (13) and the similarity measure (16). (d) Results reported in [46].
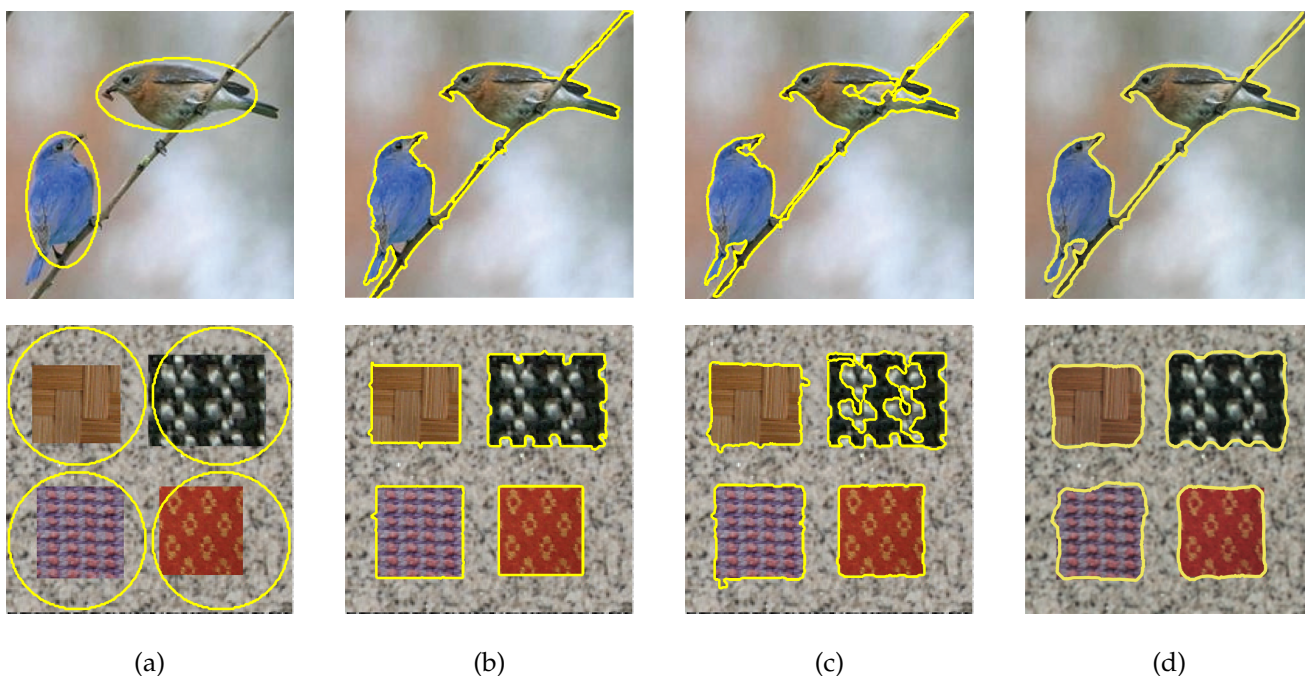

| (a) | (b) | (c) | (d) |

Fig. 11. Comparison of the proposed method (piecewise constant model, heuristic region merging) and the non-local active contour algorithm of [47]. (a) Original image with initial contours. (b) Final contour obtained with the piecewise constant model. (c) Final contour obtained with the nonlocal pairwise model (13) with the similarity measure (18). (d) Results reported in [47].
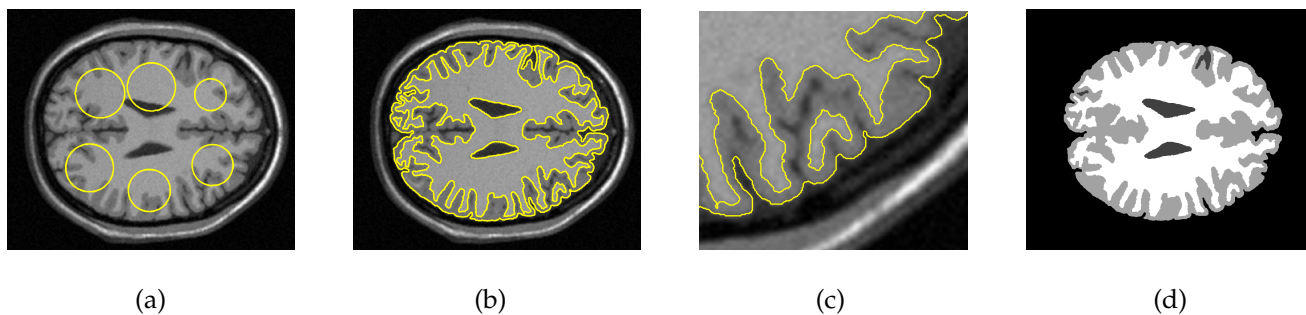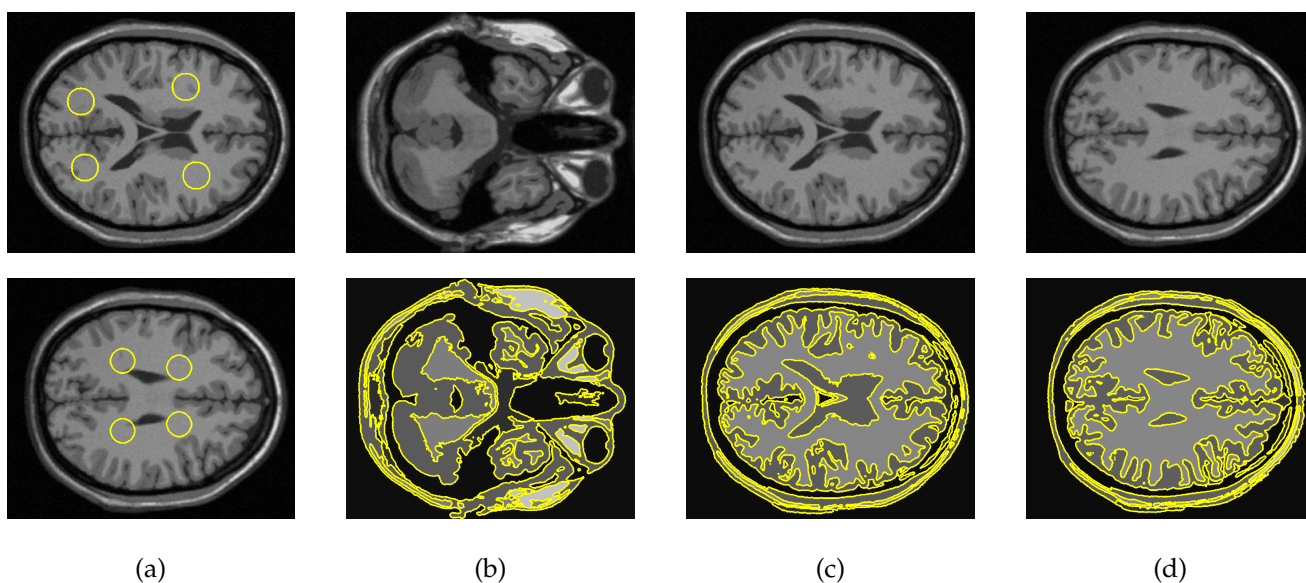
Fig. 12. Segmentation of a single MRI scan slice from the BrainWeb dataset. (a) Initial contour. (b) Final contour, (c) A closeup on the final contour. (d) The obtained regions, colored according to their mean grayscale value.

Left: two MRI slices with initial contour. Right: three slices (upper row) and the obtained segmentation (bottom row).

Exterior boundary of the white matter. Left to right: sagittal, axial, and coronal view.
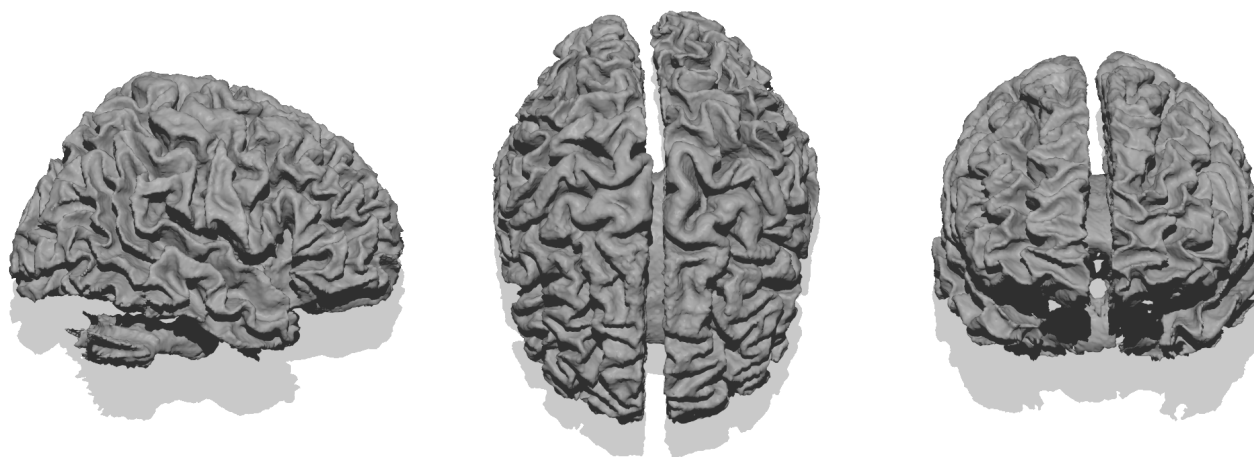
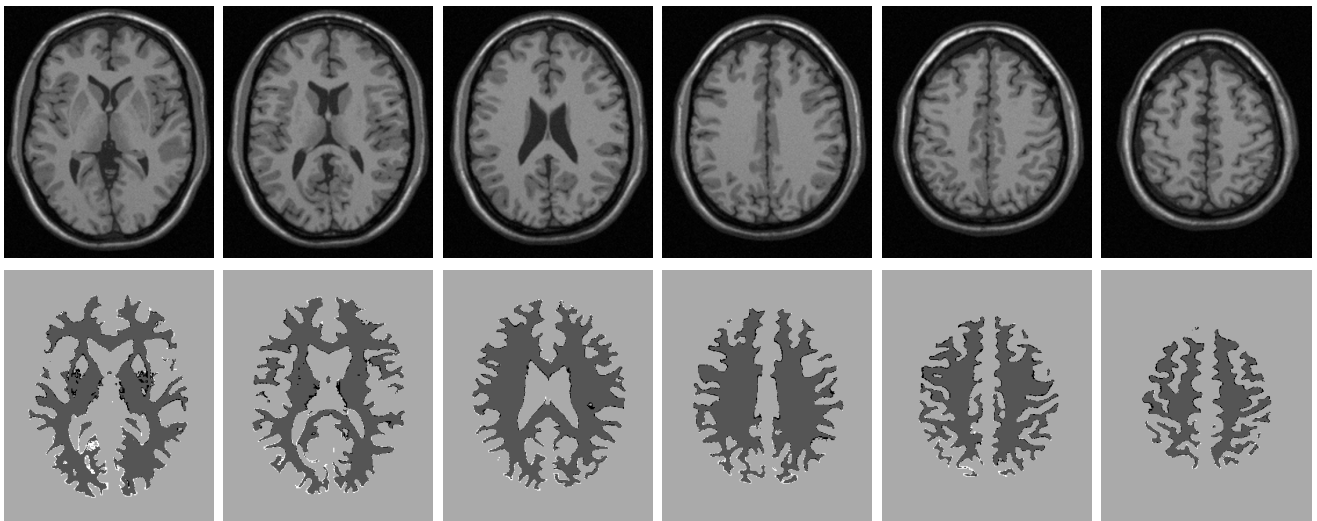Fig. 13. Segmentation of an MRI scan from the BrainWeb dataset.

Fig. 14. Comparison with the ground-truth segmentation of the white matter, from the BrainWeb dataset. Top row - original MRI image slices, bottom row - segmentation overlap, where correctly segmented pixels are shown with dark gray, pixels mistakenly labeled as the white matter region are shown with black, and white matter pixels not found by our method are shown with white.

APPENDIX

Steepest descend step minimizing the data term $E_{data}(C)$ in Eq. (13) is given by

$$C_t = -\frac{\delta E_{data}}{\delta C}$$
$$= -\sum_i \left[\int_{\Omega_i} w(x_1, x) dx_1 + \int_{\Omega_i} w(x, x_2) dx_2 \right] \mathbf{n}_i,$$

where $x \in C$, and $\mathbf{n}_i$ is the normal to C at x.

Proof: Consider a single term of the sum in Eq. (13)

$$E_i(C(t)) = \int_{\Omega_i(t)} \int_{\Omega_i(t)} w(x_1, x_2) dx_1 dx_2. \quad (43)$$

where C denotes the boundary of Ω_i. We may re-write the above functional using two auxiliary variables $\tau(t) = t$ and $t'(t) = t$

$$E_i(C(t)) = \int_{\Omega_i(\tau(t))} \int_{\Omega_i(t'(t))} w(x_1, x_2) dx_1 dx_2. \quad (44)$$

The variation of $E_i(C)$ with respect to t is given by

$$\frac{\delta E_i}{\delta C} = \frac{\delta E_i}{\delta C(\tau)} \frac{\partial \tau}{\partial t} + \frac{\delta E_i}{\delta C(t')} \frac{\partial t'}{\partial t}. \quad (45)$$

To calculate the above two functional derivatives, let us define $F(x_2, t') = \int_{\Omega_i(t'(t))} w(x_1, x_2) dx_1$. Thus, the functional $E_i(C)$ becomes

$$E_i = \int_{\Omega_i(\tau(t))} F(x_2, t') dx_2. \quad (46)$$

It was shown in [8] that the first variation of E_i as above, with respect to $C(\tau)$, is

$$\frac{\delta E_i}{\delta C(\tau)} = \frac{\delta}{\delta C(\tau)} \left\{ \int_{\Omega_i(\tau(t))} F(x_2, t') dx_2 \right\}$$
$$= -F(x_2, t') \mathbf{n}_i$$
$$= -\left[\int_{\Omega_i(t'(t))} w(x_1, x) dx_1 \right] \mathbf{n}_i. \quad (47)$$

Similarly, the first variation of E_i with respect to $\delta C(t')$ is given by

$$\frac{\delta E_i}{\delta C(t')} = -\left[\int_{\Omega_i(\tau(t))} w(x, x_2) dx_2 \right] \mathbf{n}_i. \quad (48)$$

Now, we can substitute the two last results in Eq. (45). We thus obtain

$$\frac{\delta E_i}{\delta C} = -\left[\int_{\Omega_i} w(x_1, x) dx_1 + \int_{\Omega_i} w(x, x_2) dx_2 \right] \mathbf{n}_i$$
$$= -\left[\int_{\Omega_i} (w(x_1, x) + w(x, x_1)) dx_1 \right] \mathbf{n}_i. \quad (49)$$

Finally, the first variation of the data term $E_{data}(C)$ given in Eq. (13) is

$$\frac{\delta E_{data}}{\delta C} = -\sum_{i \in N(C)} \left[\int_{\Omega_i} (w(x_1, x) + w(x, x_1)) dx_1 \right] \mathbf{n}_i,$$
$$(50)$$

which concludes the proof. □

REFERENCES

[1] M. Kass, A. Witkin, and D. Terzopoulos, "Snakes: active contour models," *IJCV*, vol. 1, no. 4, pp. 321–331, 1988.

[2] V. Caselles, F. Catté, T. Coll, and F. Dibos, "A geometric model for active contours in image processing," *Numerische Mathematik*, vol. 66, no. 1, pp. 1–31, 1993.

[3] R. Malladi, J. Sethian, and B. Vemuri, "Shape modeling with front propagation: A level set approach," *IEEE-TPAMI*, vol. 17, no. 2, pp. 158–175, 1995.

[4] V. Caselles, R. Kimmel, and G. Sapiro, "Geodesic active contours," *IJCV*, vol. 22, no. 1, pp. 61–79, 1997.

[5] D. Mumford and J. Shah, "Optimal approximations by piecewise smooth functions and associated variational problems," *Communications on pure and applied mathematics*, vol. 42, no. 5, pp. 577–685, 1989.

[6] T. Chan and L. Vese, "Active contours without edges," *IEEE-TIP*, vol. 10, no. 2, pp. 266–277, 2001.

[7] D. Freedman and T. Zhang, "Active contours for tracking distributions," *IEEE-TIP*, vol. 13, no. 4, pp. 518–526, 2004.

[8] S. Zhu and A. Yuille, "Region competition: unifying snakes, region growing, and Bayes/MDL for multiband image segmentation," *IEEE-TPAMI*, vol. 18, no. 9, pp. 884–900, 1996.

[9] N. Paragios and R. Deriche, "Geodesic active regions: A new framework to deal with frame partition problems in computer vision," *Journal of Visual Communication and Image Representation*, vol. 13, no. 1, pp. 249–268, 2002.

[10] C. Sagiv, N. Sochen, and Y. Zeevi, "Integrated active contours for texture segmentation," *IEEE-TIP*, vol. 15, no. 6, pp. 1633–1646, 2006.

[11] B. Sandberg, S. H. Kang, and T. F. Chan, "Unsupervised multiphase segmentation: A phase balancing model," *Image Processing, IEEE Transactions on*, vol. 19, no. 1, pp. 119–130, 2010.

[12] E. Bae, J. Yuan, and X.-C. Tai, "Simultaneous convex optimization of regions and region parameters in image segmentation models," in *Innovations for Shape Analysis*. Springer, 2013, pp. 421–438.

[13] Y. Boykov, O. Veksler, and R. Zabih, "Fast approximate energy minimization via graph cuts," *IEEE-TPAMI*, vol. 23, no. 11, pp. 1222–1239, Nov. 2001.

[14] C. Rother, V. Kolmogorov, and A. Blake, ""GrabCut": interactive foreground extraction using iterated graph cuts," *ACM Trans. Graph.*, vol. 23, no. 3, pp. 309–314, Aug. 2004.

[15] A. Delong, A. Osokin, H. N. Isack, and Y. Boykov, "Fast approximate energy minimization with label costs," *IJCV*, vol. 96, no. 1, pp. 1–27, 2012.

[16] J. Lie, M. Lysaker, and X.-C. Tai, "A variant of the level set method and applications to image segmentation," *Mathematics of computation*, vol. 75, no. 255, pp. 1155–1174, 2006.

[17] T. Pock, T. Schoenemann, G. Graber, H. Bischof, and D. Cremers, "A convex formulation of continuous multi-label problems," *ECCV*, pp. 792–805, 2008.

[18] T. Pock, A. Chambolle, D. Cremers, and H. Bischof, "A convex relaxation approach for computing minimal partitions," in *CVPR*. IEEE, 2009, pp. 810–817.

[19] A. Chambolle and T. Pock, "A first-order primal-dual algorithm for convex problems with applications to imaging," *JMIV*, vol. 40, no. 1, pp. 120–145, 2011.

[20] E. Bae, J. Yuan, and X.-C. Tai, "Global minimization for continuous multiphase partitioning problems using a dual approach," *International Journal of Computer Vision*, vol. 92, no. 1, pp. 112–129, 2011.

[21] D. Comaniciu and P. Meer, "Mean shift: A robust approach toward feature space analysis," *IEEE-TPAMI*, vol. 24, no. 5, pp. 603–619, May 2002.

[22] T. Cour, F. Benezit, and J. Shi, "Spectral segmentation with multiscale graph decomposition," in *Computer Vision and Pattern Recognition, 2005. CVPR 2005. IEEE Computer Society Conference on*, vol. 2. IEEE, 2005, pp. 1124–1131.

[23] P. F. Felzenszwalb and D. P. Huttenlocher, "Efficient graph-based image segmentation," *International Journal of Computer Vision*, vol. 59, no. 2, pp. 167–181, 2004.

[24] D. R. Martin, C. C. Fowlkes, and J. Malik, "Learning to detect natural image boundaries using local brightness, color, and texture cues," *Pattern Analysis and Machine Intelligence, IEEE Transactions on*, vol. 26, no. 5, pp. 530–549, 2004.

[25] P. Arbelaez, M. Maire, C. Fowlkes, and J. Malik, "Contour detection and hierarchical image segmentation," *Pattern Analysis and Machine Intelligence, IEEE Transactions on*, vol. 33, no. 5, pp. 898–916, 2011.

[26] T. H. Kim, K. M. Lee, and S. U. Lee, "Learning full pairwise affinities for spectral segmentation," *Pattern Analysis and Machine Intelligence, IEEE Transactions on*, vol. 35, no. 7, pp. 1690–1703, 2013.

[27] O. Michailovich, Y. Rathi, and A. Tannenbaum, "Image segmentation using active contours driven by the Bhattacharyya gradient flow," *IEEE-TIP*, vol. 16, no. 11, pp. 2787–2801, 2007.

[28] K. Ni, X. Bresson, T. Chan, and S. Esedoglu, "Local histogram based segmentation using the Wasserstein distance," *IJCV*, vol. 84, no. 1, pp. 97–111, 2009.

[29] A. Adam, R. Kimmel, and E. Rivlin, "On scene segmentation and histograms-based curve evolution," *IEEE-TPAMI*, vol. 31, no. 9, pp. 1708–1714, 2009.

[30] M. E. Leventon, W. E. L. Grimson, and O. D. Faugeras, "Statistical shape influence in geodesic active contours," in *CVPR*, 2000, pp. 1316–1323.

[31] D. Cremers, T. Kohlberger, and C. Schnörr, "Shape statistics in kernel space for variational image segmentation," *Pattern Recognition*, vol. 36, no. 9, pp. 1929–1943, 2003.

[32] T. Riklin-Raviv, N. Kiryati, and N. Sochen, "Prior-based segmentation by projective registration and level sets," in *ICCV*, vol. 1. IEEE, 2005, pp. 204–211.

[33] S. Osher and J. Sethian, "Fronts propagating with curvature-dependent speed: algorithms based on Hamilton-Jacobi formulations," *J. of Computational Physics*, vol. 79, no. 1, pp. 12–49, 1988.

[34] V. Caselles, R. Kimmel, and G. Sapiro, "Geodesic active contours," in *Proceedings of ICCV*. Cambridge, June 1995, pp. 694–699.

[35] V. Caselles, R. Kimmel, G. Sapiro, and C. Sbert, "Minimal surfaces: A geometric three dimensional segmentation approach," *Numerische Mathematik*, vol. 77, no. 4, pp. 423–451, 1997.

[36] H. Zhao, T. Chan, B. Merriman, and S. Osher, "A variational level set approach to multiphase motion," *J. of Computational Physics*, vol. 127, no. 1, pp. 179–195, 1996.

[37] A. Yezzi Jr, A. Tsai, and A. Willsky, "A statistical approach to snakes for bimodal and trimodal imagery," in *ICCV*, vol. 2. IEEE, 1999, pp. 898–903.

[38] C. Samson, L. Blanc-Féraud, G. Aubert, and J. Zerubia, "A level set model for image classification," *IJCV*, vol. 40, no. 3, pp. 187–197, 2000.

[39] A. Tsai, A. Yezzi Jr, and A. Willsky, "Curve evolution implementation of the Mumford-Shah functional for image segmentation, denoising, interpolation, and magnification," *IEEE-TIP*, vol. 10, no. 8, pp. 1169–1186, 2001.

[40] T. Brox and J. Weickert, "Level set segmentation with multiple regions," *IEEE-TIP*, vol. 15, no. 10, pp. 3213–3218, 2006.

[41] L. Vese and T. Chan, "A multiphase level set framework for image segmentation using the Mumford and Shah model," *IJCV*, vol. 50, no. 3, pp. 271–293, 2002.

[42] B. Lucas, M. Kazhdan, and R. Taylor, "Multi-object spring level sets (muscle)," *MICCAI*, pp. 495–503, 2012.

[43] E. Bae and X.-C. Tai, "Graph cut optimization for the piecewise constant level set method applied to multiphase image segmentation," in *Scale space and variational methods in computer vision*. Springer, 2009, pp. 1–13.

[44] R. Saye and J. Sethian, "The Voronoi Implicit Interface Method for computing multiphase physics," *PNAS*, vol. 108, no. 49, pp. 19 498–19 503, 2011.

[45] R. Saye and J. A. Sethian, "Analysis and applications of the voronoi implicit interface method," *Journal of Computational Physics*, vol. 231, no. 18, pp. 6051–6085, 2012.

[46] L. Bertelli, B. Sumengen, B. Manjunath, and F. Gibou, "A variational framework for multiregion pairwise-similarity-based image segmentation," *Pattern Analysis and Machine Intelligence, IEEE Transactions on*, vol. 30, no. 8, pp. 1400–1414, 2008.

[47] M. Jung, G. Peyré, and L. D. Cohen, "Nonlocal active contours," *SIAM Journal on Imaging Sciences*, vol. 5, no. 3, pp. 1022–1054, 2012.

[48] A. Dubrovina, G. Rosman, and R. Kimmel, "Active contours for multi-region image segmentation with a single level set function," in *Scale Space and Variational Methods in Computer Vision*. Springer, 2013, pp. 416–427.

[49] B. Sumengen and B. Manjunath, "Graph partitioning active contours (GPAC) for image segmentation," *Pattern Analysis and Machine Intelligence, IEEE Transactions on*, vol. 28, no. 4, pp. 509–521, 2006.

[50] V. Caselles, R. Kimmel, G. Sapiro, and C. Sbert, "Minimal surfaces based object segmentation," *IEEE-TPAMI*, vol. 19, no. 4, pp. 394–398, 1997.

[51] R. Goldenberg, R. Kimmel, E. Rivlin, and M. Rudzsky, "Fast geodesic active contours," *Image Processing, IEEE Transactions on*, vol. 10, no. 10, pp. 1467–1475, 2001.

[52] E. Parzen *et al.*, "On estimation of a probability density function and mode," *Annals of mathematical statistics*, vol. 33, no. 3, pp. 1065–1076, 1962.

[53] V. I. Morariu, B. V. Srinivasan, V. C. Raykar, R. Duraiswami, and L. S. Davis, "Automatic online tuning for fast gaussian summation," in *Advances in Neural Information Processing Systems*, 2008, pp. 1113–1120.

[54] G. McLachlan and D. Peel, *Finite mixture models*. Wiley-Interscience, 2000.

[55] D. Adalsteinsson and J. Sethian, "A fast level set method for propagating interfaces," *J. of Computational Physics*, vol. 118, no. 2, pp. 269–277, 1995.

[56] ——, "The fast construction of extension velocities in level set methods," *J. of Computational Physics*, vol. 148, no. 1, pp. 2–22, 1999.

[57] R. Kimmel, "Fast edge integration," Chapter in Geometric Level Set Methods in Imaging, Vision and Graphics, (S. Osher, N. Paragios, Eds.), Springer Verlag, 2003.

[58] J. Sethian, "A fast marching level set method for monotonically advancing fronts," *Proceedings of the National Academy of Sciences*, vol. 93, no. 4, p. 1591, 1996.

[59] D. L. Chopp, "Some improvements of the fast marching method," *SIAM Journal on Scientific Computing*, vol. 23, no. 1, pp. 230–244, 2001.

[60] C. A. Cocosco, V. Kollokian, R. K.-S. Kwan, G. B. Pike, and A. C. Evans, "BrainWeb: Online interface to a 3D MRI simulated brain database," in *NeuroImage*, 1997.

[61] A. Klein, J. Andersson, B. A. Ardekani, J. Ashburner, B. Avants, M.-C. Chiang, G. E. Christensen, D. L. Collins, J. Gee, P. Hellier *et al.*, "Evaluation of 14 nonlinear deformation algorithms applied to human brain mri registration," *Neuroimage*, vol. 46, no. 3, pp. 786–802, 2009.

[62] A. Vasilevskiy and K. Siddiqi, "Flux maximizing geometric flows," *Pattern Analysis and Machine Intelligence, IEEE Transactions on*, vol. 24, no. 12, pp. 1565–1578, 2002.

[63] R. Kimmel and A. M. Bruckstein, "Regularized laplacian zero crossings as optimal edge integrators," *International Journal of Computer Vision*, vol. 53, no. 3, pp. 225–243, 2003.

Guy Rosman is a Post-doctoral fellow at MIT under the Technion-MIT Post-doctoral Fellowship. He graduated in 2004 his BSc Summa Cum Laude at the Technion, and in 2008 his MSc, Cum Laude, and his PhD in 2013 at the Technion, in the Computer Science Department. During his studies, he worked at IBMs Haifa Research Labs, and in Rafael Advanced Defense Systems LTD as an algorithm developer, as well as an algorithm developer in Medicvision Imaging Solutions LTD, and Invision Biometrics. His research interests include variational and PDE based image processing, as well as inference methods and algorithms for motion and structure estimation.

Ron Kimmel is a Professor of Computer Science at the Technion where he holds the Montreal Chair in Sciences. He held academic positions at UC Berkeley and Stanford University. He has worked in various areas of image and shape analysis in computer vision, image processing, and computer graphics. Kimmel's interest in recent years has been non-rigid shape analysis, medical imaging and computational biometry, numerical optimization of problems with a geometric flavor, and applications of metric and differential geometries. Kimmel is an IEEE Fellow for his contributions to image processing and non-rigid shape analysis. He is the founder of the Geometric Image Processing Lab. and a founder and advisor of several successful image processing and analysis companies..

Anastasia Dubrovina received the BSc and the MSc degrees in Electrical Engineering from the Technion - Israel Institute of Technology, Haifa, Israel. She is currently working towards the PhD degree in Computer Science at the Technion. Her research interests include image segmentation, variational methods, 3D shape matching and spectral shape processing.